Areal detection efficiency of channel electron multiplier arrays*

J. A. Panitz and J. A. Foesch

Sandia Laboratories, Albuquerque, New Mexico 87115

(Received 4 April 1975; in final form, 5 May 1975)

The areal detection efficiency of a channel electron multiplier array (CEMA) and the nature of its secondary emission surface were investigated with the ion microprobe mass analyzer (IMMA). Previous speculations of detection efficiency based on simple geometric arguments of channel-to-interchannel area ratios are shown to be in error. With a positive bias applied to a front electrode surface of high secondary yield, areal detection efficiency of a CEMA may approach 100% even for single-ion impacts. The secondary emission properties of a CEMA are shown to be determined by an alkali-rich surface layer on each channel wall, and not a concentration of Pb or PbO as previously thought. Both reversible and irreversible gain degradation observed when heating a CEMA in vacuum are interpreted as a change in the composition of this layer.

The channel electron multiplier array (CEMA) is a versatile particle detector providing a large active area of high gain which is unaffected by repeated exposure to the atmosphere.[1] Despite its wide use for ion, electron, and photon detection,[2–5] little detailed information exists as to its areal detection efficiency or even the related nature of its active secondary emission surface. This is surprising since areal detection efficiency is of prime importance when using a CEMA for single ion counting, particularly when counting statistics are limited, as in single-atom mass spectrometers such as the atom-probe[6] or field desorption spectrometer.[7] One might reasonably assume that only ions striking the individual channels of the CEMA would have a high probability of detection,[8,9] since it could be argued that the production and collection of secondary electrons produced by ion impacts between channels are small. If correct, such an argument would limit the areal detection efficiency to the fraction of the surface area occupied by channels[8,9] (the open area ratio, OAR) which, for a typical CEMA (37 μ channels on 50 μ centers), would be only 58% of the total area. The structural integrity of the array would then provide an upper limit to areal detection efficiency since a CEMA with an OAR greater than 70% would be too fragile to manufacture. As a consequence, it would be impossible to detect every particle striking a CEMA and therefore impossible to achieve the stated objective of the atom probe[10] and the expected utility of the field desorption spectrometer.[11]

In this paper we will describe the first direct measurement of the areal detection efficiency of a typical CEMA exposed to a nanoampere beam of positive ions and indicate from a computer simulation how the detection efficiency may approach 100% for single-ion impacts. By mass analyzing the secondary ions produced at the CEMA surface by the primary nanoampere beam as a function of beam position, we will also obtain two-dimensional species distributions which will characterize, for the first time, the secondary emission surface of a CEMA. Finally, by using the primary ion beam to sputter the CEMA surface, we will obtain depth profiles of active species in the near-surface region and show how the results can be used to explain the gain degradations produced by heating a CEMA in vacuum at elevated temperatures.

APPARATUS

In order to analyze a CEMA under operating conditions, a commercial ion microprobe (IMMA)[12] was modified to accept, on its sample carrousel, a CEMA[13] mounted in a manner similar to that described previously.[14] The potentials of the front (V_f) and back (V_b) surfaces of the CEMA, as well as the collector (V_c), could be independently varied. Since the CEMA collector could not be observed during operation, a phosphor screen was not used, and, therefore, the CEMA output could not be visually recorded. Figure 1 schematically shows the essential features of the apparatus since the IMMA itself has been described in great detail elsewhere.[15] The primary, 20 kV ion beam (N_2^+ and Ar^+ were used) was focused at the CEMA surface to a diameter of 2μ, which was smaller than any characteristic dimensions of the array. A raster circuit in the IMMA could move the beam across the CEMA in one or two dimensions. Since the sample carrousel holding the CEMA could be precisely translated (with micrometer accuracy) independently in two dimensions or rotated about its axis, any CEMA hole orientation relative to the primary beam sweep could be obtained. As Fig. 1 indicates, an x-gain

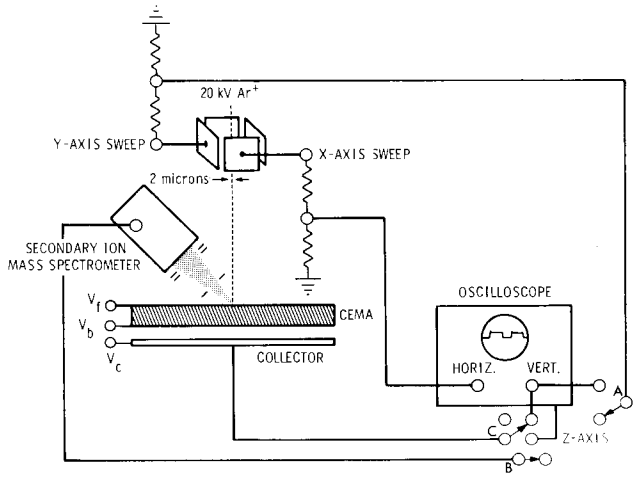

FIG. 1. Schematic of the ion microprobe (IMMA) and CEMA used for this study.

profile could be obtained by connecting the collector signal (C) of the CEMA to the vertical input of the oscilloscope, the horizontal input synchronized to the primary beam sweep. A two-dimensional ($X-Y$) gain profile was generated by connecting the y-axis sweep signal (A) to the vertical amplifier and the z-axis modulating the beam intensity with the collector signal (C) so that the trace would become brighter as the CEMA output increased. The mapping of a given species location on the surface was accomplished by tuning the secondary ion mass spectrometer to the described mass and modulating the oscilloscope beam intensity, whose position was again synchronized with that of the primary beam. A conventional mass spectrum could be obtained by fixing the primary beam position and sweeping the secondary ion mass spectrometer from mass 1.0 to 200, with its output connected to the vertical amplifier of the oscilloscope, or a chart recorder whose x sweep was synchronized to the mass sweep itself. Depth profiling was obtained by tuning the mass spectrometer to a given species and recording the change in output signal as the primary ion beam, fixed at a given position on the surface, sputtered through the near-surface region. A cryobaffle and ion pump kept the IMMA background pressure at the sample in the 10^{-7} Pa range. With the primary ion beam rastering the CEMA surface, the pressure was always below 1×10^{-4} Pa.

Figure 2(a) is an optical photomicrograph of the CEMA surface showing the width and extent of the primary beam sweep taken after the x-gain profile of Fig. 2(b). To obtain the visible mark on the evaporated chrome electrode surface, the beam was swept in the x direction, to the extent indicated, for several minutes. As can be seen, the sweep passes over three channels and two interchannel spaces. In this case, the channels are inclined 15° to the surface normal (15° bias), with the CEMA oriented so that the primary beam sweeps almost perpendicular to channel bias direction. With $V_f = -1500$ V, $V_b = -500$ V, and the collector connected to the 1 MΩ y input of the oscilloscope ($V_c = 0$), the gain profile of Fig. 2(b) was generated. The zero baseline is shown from which relative gains can be obtained; the greater the displacement of the trace from the baseline, the higher the gain. At point A, the primary beam has just entered the center channel in the sweep path of Fig. 2(a). The gain decreases rapidly to a constant value as the beam sweeps across the channel wall at a constant depth from the CEMA surface, well within the channel. At point B, the beam begins to traverse an interchannel area, and at C it enters the left-hand channel in Fig. 2(a). The increase of gain at points A and C results from the primary beam striking the channel wall near the CEMA surface, allowing the secondary electrons within the channel to make more impacts with the channel wall before emerging. A surprising observation is that the interchannel area exhibits appreciable gain which is only slightly less than that observed for ion impact at a channel entrance. This result clearly indicates that the simple open area ratio description of areal detection efficiency is incorrect since it assumed zero detection efficiency in the interchannel area. Although Fig. 2(b) was obtained by scanning a 5° plate, the same trends were observed for a 15° biased plate oriented in an identical manner with respect to the primary beam sweep. To obtain the relatively symmetric traces of Fig. 2(b), it was necessary to sweep once rapidly across the path shown in Fig. 2(a). Successively sweeping or making a single sweep of long duration caused the trace amplitude to become randomly erratic, an observation consistent with the effect of channel fatigue reported previously.[16]

The CEMA gain profile can be presented more graphically by rastering the primary beam in two dimensions across the CEMA surface. With the oscilloscope beam synchronized to the position of the ion beam at the surface and its intensity modulated by the CEMA output (greater intensity equals higher gain), the two-dimensional gain profile of Fig. 3 is obtained. Image

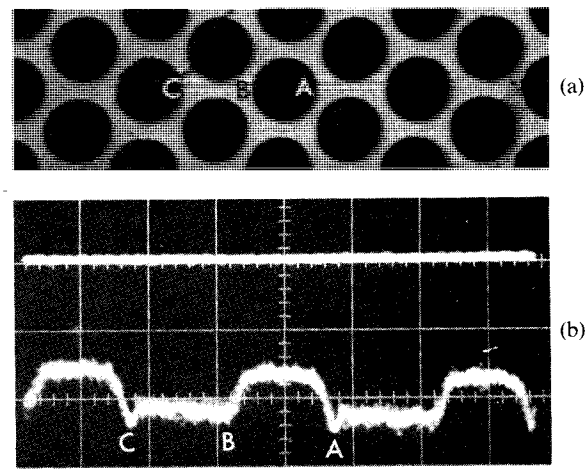

FIG. 2(a). Optical micrograph of CEMA surface showing the line scanned for the x-gain profile of Fig. 2(b). 37 μ channel diameter, 50 μ center-to-center channel spacing.

FIG. 2(b). x-gain profile of CEMA (5° bias). $V_f = -1500$ V, $V_b = -500$ V, $V_c = 0$(5×10^{-10} A, 20 kV, Ar^+). Zero baseline is shown.

contrast was adjusted so that the region of smallest gain appears darkest. The highest gain (brightest) region occurs nearest the channel entrance as expected, with the interchannel area exhibiting slightly less gain. One would expect, because of the bias angle of the channel, a gradual reduction in gain as the primary beam penetrates deeper within the channel, until it clears the channel entirely. What is observed for each channel in Fig. 3 is a very bright and a very dark region, the gradual change in brightness masked by the image contrast. The reason for the area of reduced gain within the high gain region is not clear, but since it appears at an identical location with respect to each channel, it is probably due to a systematic change in the secondary emission properties of the channel wall. Such a variation could be due to electrode material deposited on the channel wall during CEMA manufacture, a condition which would also make the channel outlines in Fig. 3 less than circular. However, the important conclusion resulting from Figs. 2 and 3 remains independent of such considerations: the areal detection efficiency of a CEMA is not limited to the fraction of the total area occupied by the individual channels, but includes an appreciable fraction of the interelectrode area as well.

Let us consider the conditions necessary for the interchannel area to exhibit gain and, therefore, the areal detection efficiency to be large. Obviously, the primary ion beam must first produce secondary electrons which in turn must be collected in neighboring channels, since only within a channel can the multiplication process occur. To be efficient, the collection process requires that the electric field at the surface direct the secondary electrons into neighboring channels with high probability, and since the electric field is a function of front surface bias, V_f,[17] the collection (or areal detection) efficiency will be a function of V_f. For example, one would expect that for the large, negative bias used to obtain Figs. 2(b) and 3(a) the detection efficiency would be smaller than for a zero or small positive bias, since a large negative bias would discourage secondaries from entering neighboring channels. To measure the relative gain change as a function of V_f it is necessary to change V_f while keeping the total potential difference across the CEMA constant. Since it was necessary to observe the effect of a zero or small positive bias, the CEMA collector potential, V_c, had to be maintained at a high positive potential with respect to ground. This in turn required capacitively coupling the collector to the oscilloscope input, which meant that relative gains determined by measurements from a zero baseline could not be made as in Fig. 2(b). Instead, only changes in the peak-to-peak amplitude of the gain signal of Fig. 2(b) could be determined as a function of V_f. To display the results more graphically, an $X-Y$ gain profile was again generated by rastering the primary beam over an area of the surface large enough to display the symmetry in the placement of the individual channels. The oscilloscope sweep was moved in synchronization, with its beam intensity modulated by the output of CEMA, producing a picture of the CEMA surface with the brightness of a region proportional to its gain. With the front surface biased at zero, the contrast of the image was adjusted so that the channels appeared dark. A change in the bias should then produce a change in the brightness of the interchannel area proportional to the change in collection efficiency. Figure 4 shows the results for five different values of V_f ranging from -10 to $+10$ V, with 1000 V maintained across the CEMA. Photographic development times were the same for each photograph, all of which were obtained from the same roll of Polaroid film. As can be seen, the effect of making V_f more positive was to increase the gain in the interchannel area. Contrast variations were difficult to observe for $V_f > 10$ V so that it was not possible to obtain an optimum value for V_f with any precision. However, the results did indicate that $V_f > 10$ V produced the best detection efficiency in the interchannel areas.

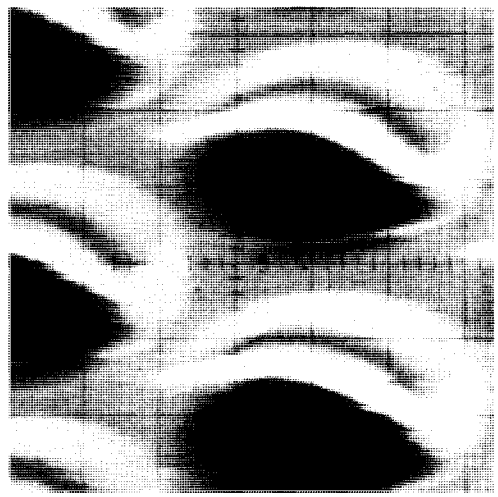

FIG. 3. Gain profile of CEMA (5° bias). $V_f = -1500$ V, $V_b = -500$ V, $V_c = 0$. ($<1.0 \times 10^{-9}$ A, 20 kV, Ar^+). See text for relation of intensity to gain.

In order to determine the effect of CEMA parameters on areal detection efficiency, a computer code[18] was used to calculate the trajectories of secondary electrons emitted from a point on the front CEMA surface within the interchannel area. The simulation was performed as a function of initial electron energy (1.5–4.5 eV), the dielectric constant of the CEMA (1.0–9.0), and the potential applied to the front surface, V_f (0–90 V). Thirty-seven μ channels on 50 μ centers were used to model the CEMA surface, the channels inclined 5° to the surface normal. For the simulation, 1000 V was applied across the CEMA with ground approximately three channel diameters from the front surface of the CEMA. The results followed the trend of Fig. 4. The collection efficiency improved with increasing positive bias, until at $V_f \cong 22$ V all secondary electrons with energies between 1.5 and 4.5 eV emitted from any point between two channels up to ±45° from the surface normal were

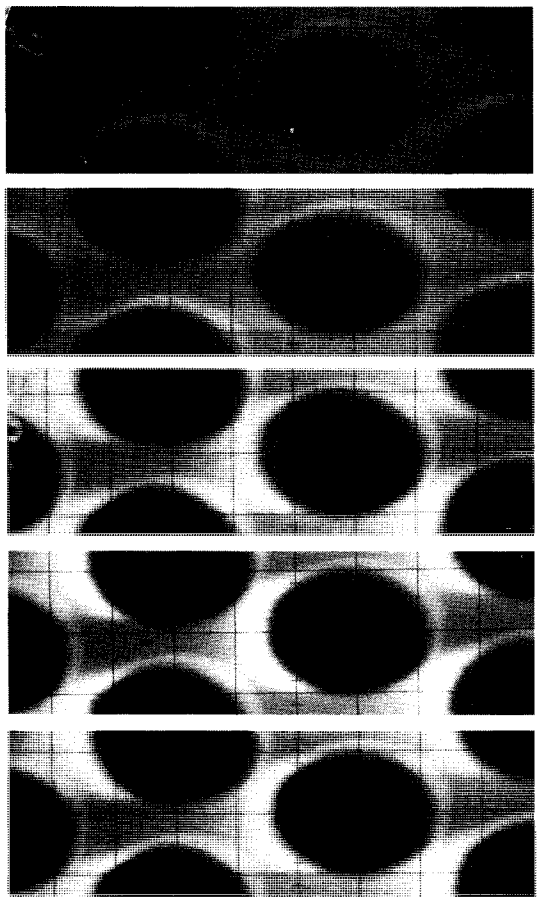

FIG. 4. $(X-Y)$ ac gain profile of CEMA (output capacitively coupled to oscilloscope). From top (darkest) to bottom: $V_f = -10$ V, -3 V, 0, $+3$ V, $+10$ V. $(V_b - V_f) = 1000$ V, $V_c = 1500$ V (5° bias).

collected. At smaller, positive bias, most secondaries were collected, but usually several channels distant from the emission site. At large positive biases ($V_f \cong 90$ V), the secondaries were returned to the interchannel area in the immediate vicinity of the point of emission, so that collection efficiency was drastically reduced. Large negative biases removed most of the secondaries from the CEMA surface (even at the channel entrances) also producing a small detection efficiency and an overall decrease in gain. An intriguing result of the simulation was the general insensitivity of the electron trajectories to the dielectric constant of the CEMA, even with $\epsilon = 1.0$ (equivalent to entirely removing the glass capillary array from between the CEMA electrode surfaces). The implication is that at least for discussions of the interchannel collection efficiency, the CEMA may be treated as two plates at potential V_b and V_f containing multiple apertures, and it is the electrostatic lens properties of the front plate at potential V_f, and not any other CEMA characteristic, which determines the collection efficiency of secondary electrons.

Figure 5 is a tracing of the trajectories and several equipotentials generated by the computer for the specific case of $V_f = 22.5$ V, with an initial electron energy of 3.5 eV and a dielectric constant, $\epsilon = 4.5$. Since the trajectories are, at least to first order, the same when using a dielectric constant of 1.0, one can assume that the bias angle of the CEMA has no effect on the collection efficiency from the interchannel area. However, the bias angle does effect the overall gain of the CEMA since a shallower bias cut (5° instead of 15°) permits the impacting secondaries to travel further into the channel before striking the walls and initiating the multiplication process.

From computer simulation and IMMA measurements we can specify the two conditions which, for any CEMA having 37 μ holes on 50 μ centers, will maximize areal detection efficiency:

(1) The application of an empirically determined positive bias to the front electrode surface (from this study determined to be approximately 22 V).

(2) The use of a suitable material having low resistivity and high secondary electron yield (for example, BeCu) for the CEMA front surface electrode. A material such as gold is ideal for the back electrode since it minimizes ion feedback by discouraging gas adsorption, and is a good choice for a front surface electrode if maximum areal detection efficiency is not required.

Under such conditions, areal detection efficiency (and gain) of a CEMA will be controlled by the depth at which incident particles strike the channels, at least for particles striking the CEMA surface at normal incidence. For small (or zero) bias angles such particles will strike the channel wall deep within the channel producing little (or zero) gain. One comment is in order when applying the results of IMMA measurements of areal detection efficiency to single-ion counting experi-

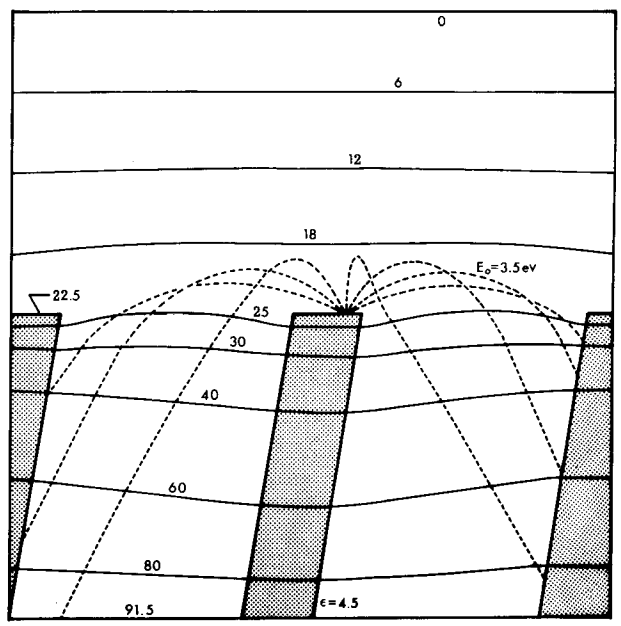

FIG. 5. Computer simulation of CEMA (5° bias). $V_f = 22.5$ V, $(V_b - V_f) = 1022.5$ V. 37 μ channel diam, $\epsilon = 4.5$, initial secondary electron energy -3.5 eV. Plot has been compressed in vertical dimension ($\approx 2\times$) for convenience. Values of selected equipotentials are shown, with ground approximately three channel diameters from the CEMA front surface.

TABLE I. CEMA ion species. The species are typical of those observed during a CEMA mass scan, with the chromium species characteristic of the vapor-deposited front surface electrode. The composition of Corning 8161 glass (parts by weight) is typical of the composition of glass used in CEMA manufacture.

IMMA ion species	Corning 8161 glass
Si^+	SiO_2 (39%)
Pb^+	PbO (51.5%)
Na^+	Na_2O (0.2%)
K^+	K_2O (5.1%)
Rb^+	Rb_2O (2.0%)
Cs^+	Cs_2O (0.2%)
Ba^+	BaO (1.5%)
...	As_2O_3 (0.5%)
Cr^+	

ments. In the IMMA experiments, a beam current of 10^{-10} A was normally used so that the number of ions striking the CEMA at any time during the sweep was large. Therefore, even if only 20% of the incoming ions produced secondary electrons, and only 10% of these were collected, the gain would still be large. This is the most probable explanation for the reasonable interchannel area gain of Figs. 2(b) and 3(a) where $V_f = -1500$ V, consistent with the computer simulation which predicted a small interchannel area gain under such biasing conditions. For single-ion counting, provided the optimum operating conditions described above are realized (secondary electron yield is greater than one, $V_f \approx 22$ V but is optimized empirically, and the bias angle is reasonable, $\approx 15°$), areal detection efficiency approaching 100% should be possible.

It is interesting to compare this study of areal detection efficiency with previous measurements by Burroughs[9] using photoelectrons at normal incidence. It is not surprising that he observed an efficiency of only 76%, since the evaporated electrodes of his specially prepared CEMA had a secondary electron coefficient less than one,[9] and bombardment by more massive ions (known to increase the secondary yield[19]) was not attempted. Probably more important, however, was that the front electrode penetrated unusually far (four channel diameters) into each channel. This would effectively minimize potential variations at the channel entrance, reducing the field penetration necessary for the efficient collection of secondaries from the interchannel area. Although the bias angle of the CEMA was not given, Fig. 2[9] would suggest that it was zero, further reducing collection efficiency. The collection efficiency of a CEMA is appreciably reduced for particles at normal incidence when its bias angle is zero, since a large fraction of the incident particles can pass through the channels without striking a channel wall.

In order to identify the surface species responsible for the secondary emission properties of a CEMA, a channel wall was bombarded by the primary IMMA ion beam while the secondary ions produced were identified by the mass spectrometer. The resulting characteristic species are given in Table I. Following sputtering of the region, the expected Pb^+ species was observed. Upon checking,[20] it was discovered that the composition of Corning 8161 glass[21] is typical of that used in CEMA manufacture. Table I shows its composition with the numbers in parentheses referring to constituent parts by weight. The oxides were not observed, probably because of the usual problem of observing them when sputtering with argon. Unfortunately, the IMMA could not easily provide absolute or even relative species abundance because of the variation in secondary yield for the different species. Spectra obtained in the interchannel area showed Cr^+ (the front surface electrode material was chromium) until a crater exposed the underlying substrate by the sputtering process. Then the species shown in Table I were again detected.

To determine the location of the alkali species on the surface, the IMMA was operated in its $(X - Y)$ raster mode. With the secondary ion mass spectrometer turned to the desired mass and its output modulating the intensity of the oscilloscope sweep synchronized to the primary beam position, the two-dimensional distribu-

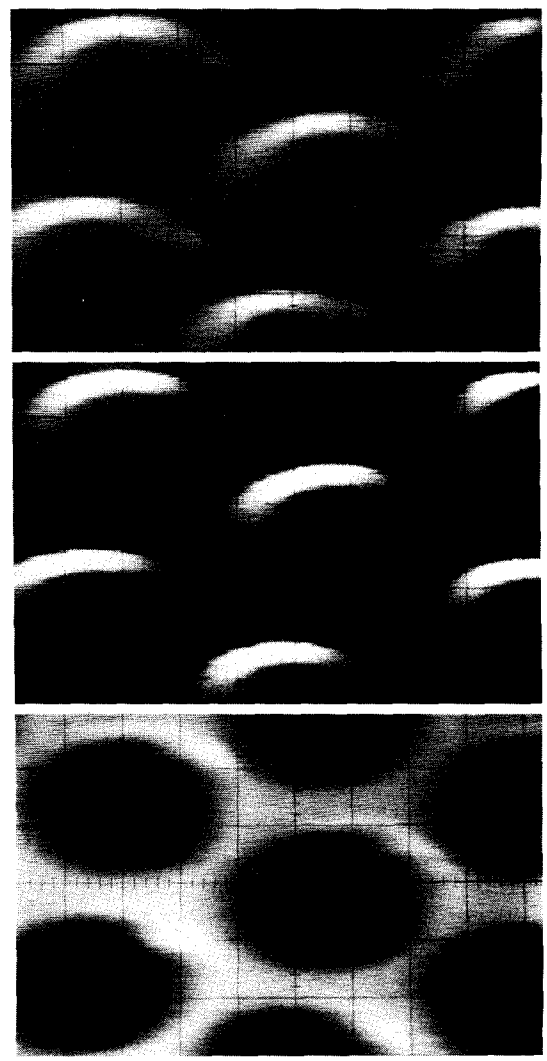

FIG. 6. CEMA species distributions. Na^+ (upper), Rb^+ (middle), Cr^+ (lower). $V_f = V_b = +1460$ V, 5° CEMA bias.

tions shown in Fig. 6 were obtained. As expected, the Cr^+ species appeared primarily in the interchannel area with only a small indication (from the less than circular shape of the channel perimeter) of penetration into the channels. The Na^+ and Rb^+ distributions appear as crescents at essentially the same location along the perimeter of each channel, indicating that these species line the channel walls. The distribution over the entire channel was not obtained since the 5° bias would prevent secondary ions from leaving the channel in the region where primary beam penetration was even one channel diameter deep. During such scans, both CEMA electrodes were maintained at the same, constant potential ($V_f = V_b = +1460$ V) to encourage secondary ion collection at the mass spectrometer entrance aperture. Similar distributions were obtained for K^+, Ba^+, and Li^+, but no appreciable Pb^+ signal was observed until some sputtering of the region was accomplished. Although the sputtering yield was expected to be much smaller for Pb^+ than for the alkali species, the observations indicated that Pb^+ was located beneath a surface-rich alkali (oxide) layer. To examine this possibility further, the height of the K^+ mass peak was monitored as a function of time during which a small (2 μ diam) region of the channel wall was sputtered. The resulting depth profile showed a large concentration of K^+ at the surface, followed by a rapid decrease in abundance and then a smaller increase to a level which did not change with time. A very crude comparison with the Cr^+ profile obtained while sputtering through the $\approx$200 nm electrode layer in an interchannel area showed that the surface-rich K^+ region was about 150 nm thick, with the following depletion region about 600 nm in extent. Although several of the other alkali species were also examined in this manner, only K^+ exhibited such a marked variation with depth. Such a profile can be explained by assuming that during manufacture, the heat treatment of the CEMA in hydrogen causes a preferential segregation of the mobile alkali species to the surface leaving an alkali depleted region as a transition to bulk concentration. Subsequent atmospheric oxidation of the surface layer then produces the active surface responsible for high secondary multiplication yields. PbO, which is the major constituent of the starting material, is partially reduced by the same heat treatment to form Pb clusters responsible for the color and resistivity of a CEMA but not its secondary multiplication properties. A surface-rich alkali-oxide layer may explain the irreversible gain decrease observed when a CEMA is heated in vacuum to 250°C.[22] At such a temperature the volatile alkali species would desorb from the surface, and since species migration from the bulk would be slow, the gain of the CEMA would not appear to recover. Moderate vacuum bakes reported to reversibly reduce CEMA gain[22] probably result from decomposition of the alkali oxides without their total removal from the surface. Reexposure of the CEMA to the atmosphere for a sufficient length of time would result in reoxidation and an increase in gain to the nominal value obtained prior to the vacuum bake.

ACKNOWLEDGMENTS

The authors wish to thank R. J. Walko for many helpful discussions, J. E. Boers for his assistance with the computer simulation, and R. L. Pierle and L. D. Owens of Galileo Electro-Optics for providing the CEMAs used in this study.

* This work supported by the U.S. Energy Research and Development Administration.

[1] D. Washington, Nucl. Instrum. Methods **3,** 573 (1973).
[2] P. J. Turner, P. Cartwright, M. J. Southon, A. Van Oostrom, and B. W. Manley, J. Phys. E. **2,** 731 (1969).
[3] E. L. Thomas and S. Danyluk, J. Phys. E **4,** 843 (1971).
[4] R. Lewis and R. Gomer, Appl. Phys. Lett. **15,** 384 (1969).
[5] S. S. Brenner and J. T. McKinney, Rev. Sci. Instrum. **43,** 1264 (1972).
[6] E. W. Müller, Naturwissenschaften **5,** 222 (1970).
[7] J. A. Panitz, J. Vac. Sci. Technol. **11,** 206 (1974).
[8] E. G. Burroughs, Rev. Sci. Instrum. **40,** 35 (1969).
[9] R. J. Walko and E. W. Müller, Phys. Status Solidi **9** (9), K9 (1972).
[10] E. W. Müller, J. A. Panitz, and S. B. McLane, Rev. Sci. Instrum. **39,** 83 (1968).
[11] J. A. Panitz, *Proceedings of the Hydrogen Economy Miami Energy (THEME) Conference* (Plenum, New York, 1975)
[12] Ion microprobe mass analyzer (IMMA) manufactured by Applied Research Laboratories, Glendale, CA.
[13] Supplied by Galileo Electro-Optics (formerly Bendix Electro-Optics), Galileo Park, Sturbridge, MA.
[14] J. A. Panitz, Rev. Sci. Instrum. **42,** 724 (1971).
[15] T. A. Whatley, C. B. Slack, and E. Davidson, 6th International Conference on X-ray Optics and Microanalysis, Osaka, Japan, Sept. 1971, p. 417.
[16] A. Seko and H. Kobayashi, Rev. Sci. Instrum. **44,** 400 (1973).
[17] For the CEMA experiments, the grounded cryobaffle of the IMMA, located parallel to the CEMA surface and approximately 3 cm away, served to terminate the field generated by V_f.
[18] J. E. Boers, J. Vac. Sci. Technol. **10,** 1120 (1973).
[19] K. Krebs, Fortschr. Phys. **16,** 419 (1968).
[20] R. L. Pierle, Galileo Electro-Optics (private communication).
[21] R. H. Dalton and G. B. Hares, US Patent No. 2,964,414, Table II, ex. 23 and 24 (1960).
[22] J. P. Rager, J. F. Renaud, and V. Tezenas du Montcel, Rev. Sci. Instrum. **45,** 927 (1974).